Int. J. Electrochem. Sci., 16 **(2021)** Article Number: 211057, doi: 10.20964/2021.10.48

International Journal of
ELECTROCHEMICAL
SCIENCE
www.electrochemsci.org

CFD simulation and investigation of a new radial flow field structure on the PEMFC circular bipolar plate

Qizhen Xie[1], *Yutao Lian*[2], *Minggang Zheng*[1*]

[1]School of Mechanical and Electronic Engineering, Shandong Jianzhu University, Jinan 250101, Shandong, PR China
[2]School of Automotive Studies, Tongji University, 4800 Caoan Road, Shanghai, 201804, China
[*]E-mail: why1318@sdjzu.edu.cn

Received: 30 June 2021 / *Accepted:* 18 August 2021 / *Published:* 10 September 2021

Proton exchange membrane fuel cells (PEMFCs) have received considerable attention in recent years as an efficient method of utilizing hydrogen energy. In PEMFCs, the bipolar plate is an important component, and flow channel design plays an important role in reaction gas distribution and product removal. Based on the circular bipolar plate structure, a new radial flow channel design scheme is proposed in this paper. This scheme adopts a central inlet method, where the gas enters from the center of the flow field and then diffuses around, and the adjacent flow channels transfer the reaction gas and products through the holes located in the middle of the ribs. The number of rib floors and the number and arrangement of holes on each rib floor are selected as the key variables of this structure, and PEMFC monomer models with differences in the above variables are established and then simulated by the CFD method. After a comparative analysis of the difference in oxygen distribution, water removal and cell output performance of each scheme, a comprehensive optimal design for this radial flow channel structure is finally proposed.

Keywords: Proton exchange membrane fuel cell; circular bipolar plate; radial flow channel; CFD simulation

1. INTRODUCTION

To address environmental pollution and fossil fuel depletion, governments and institutions of various countries have carried out a considerable number of research studies and applications for new energy technologies [1]. Among the many new energy sources, hydrogen energy is regarded as the most promising clean energy source in the 21st century, and research on hydrogen energy has been carried out in many countries and regions around the world since the 1970s. As the main method of utilizing hydrogen energy, the proton exchange membrane fuel cell (PEMFC) uses hydrogen as the anode fuel to

generate electricity through a chemical reaction with oxygen at the cathode. It has the advantages of low operating temperature, no pollution (the product is only water), low noise, and high energy conversion efficiency [2]. As an important component of PEMFCs, the optimization of bipolar plates can notably improve the output performance of fuel cells, which is significant for the commercialization of hydrogen energy and fuel cells. The improvement of flow channel structures and corresponding parameters has been a main focus of bipolar plate research. The above two factors can help the reaction gas to fully distribute into the membrane to participate in the electrochemical reaction, thereby improving the performance of fuel cells, and they can also promote the discharge of the liquid water generated by the reaction from the flow channels in a timely and efficient manner to ensure the reliability of fuel cell operation [3-5].

In addition to the improvement of traditional structures such as straight flow channels [6, 7] and serpentine flow channels [8, 9], the optimization of the radial flow channels on the circular bipolar plates has also been a research focus in recent years. Compared with the conventional structures, the radial flow channel structure adopts a central inlet arrangement in which the gas enters from the inlet located at the center of the flow field and then diffuses in all directions along flow channels, and finally exits through the outlets distributed at the edges of the circular bipolar plate.

Diethelm [10] first proposed the circular bipolar plate and applied it to the solid oxide fuel cell, and they claimed that this structure could effectively solve the problem of bipolar plate fragility during the assembly of the fuel cell stack. Batawi [11] adopted the circular bipolar plate in a high-temperature fuel cell stack and for the first time integrated the exhaust gas treatment unit responsible for the post-combustion process on the plate, which greatly reduced the manufacturing cost and the space occupied. However, the flow channel structure on the circular bipolar plate was not specifically optimized in the earlier designs proposed by Diethelm or Batawi. For this reason, Schuler [12], Doggwiler [13, 14] and others optimized the flow channel structure in their proposed fuel cell stacks, respectively. In order to improve the fluid transport capacity on the cathode side, Schuler used circular bipolar plates with a labyrinth-like flow channel structure in his scheme and confirmed the superior performance of this structure in terms of gas transport, distribution, and tail gas emission through subsequent studies. Doggwiler, on the other hand, used the pin flow channel structure in his scheme and compared it with the labyrinth-like flow channels. The results showed that the pin flow channel structure also had an excellent gas transport performance.

Research on improving the flow channel structure through the whole fuel cell stack introduced in the above-mentioned literature is costly and time-consuming, and has high safety risks. Therefore, most of the current research on the radial flow channel structure has focused on fuel cell monomers. Hernandez-Guerrero [15] and Friess [16] established PEMFC single models with different radial flow channel structures and then simulated, respectively. All simulation results showed that the radial flow channel structure was better than the conventional flow channel in terms of water concentration, cathode gas and current density distribution. Vladimir [17] combined the characteristics of the radial flow channel structure and the interdigital flow channel structure. Although this design improved the mass transfer effect, it also produced a larger pressure drop. In contrast, the radial flow channel structure proposed by Perez [18] avoided large pressure drops, however, such structures were too complex and presented water removal and pressure distribution problems when one of the outlets was blocked by

water. Solati [19] took a different approach, he investigated the effects of the different CL, GDL and membrane arrangements on the radial flow channel structure in PEMFCs, then proposed an optimization approach for all three of them based on their findings.

Although some progress has been made in the study of radial flow channels for fuel cells, there are still more problems that need to be solved. Therefore, such flow channel structures still have important research significance and broad development prospects. Based on a thorough investigation of previous literatures, a new radial flow channel structure on circular bipolar plates is proposed in this paper. In this structure, the number of rib floors and the number and arrangement of holes on the different ribs are selected as the key variables. In order to explore how these two key variables affect the performance of radial flow channel structures, PEMFC models with different arrangements of the variables mentioned above are established and then simulated through the CFD method. The ultimate aim of this study is to propose a comprehensive optimization scheme for this radial flow channel structure by comparing and analyzing different simulation results in terms of water distribution, oxygen distribution and cell output performance.

2. NUMERICAL MODEL AND METHOD

2.1. Modeling

The proposed circular bipolar plate with a radial flow channel structure is shown in Figure 1(a). This structure adopts the central inlet method and mainly consists of two parts: flow channels and ribs. The flow channel is used for the reaction gas and product flow. The ribs are connected to the adjacent flow channels by holes located in their middle instead of the grooves located on the upper part, and this characteristic also plays a crucial role in the evacuation of gas and product. After analyzing the flow characteristics of the fluid within this structure, we believe that the number of rib floors and the number and arrangement of holes on the different ribs can have a significant impact on the performance of such flow channel structures. In order to verify such viewpoints, this work proposes a large number of comparison schemes with the different variables mentioned above. According to these schemes, the complete PEMFC monomer models as shown in Figure 1(b) are established and then simulated by the CFD method. It should be mentioned that during the simulation, one quarter of the complete model is used as the computational domain in order to facilitate the calculation. The main geometric parameters used in the construction of the model are shown in Table 1.

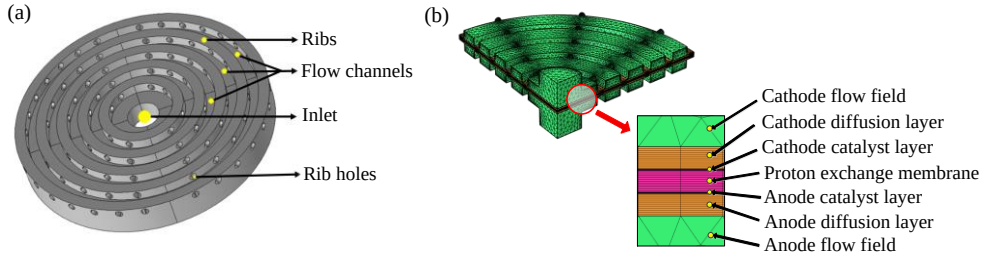

Figure 1. (a) Structure of the radial flow channels and (b) computational domain used by CFD

Table 1. Main geometrical parameters

Parameter	Value	Unit
Rib width/depth	1×10^{-4}/ 1×10^{-4}	*m*
Outermost circular radius of the radial flow channel	1.805×10^{-3}	*m*
Thickness of the GDLs	0.19×10^{-4}	*m*
Thickness of the MPLs	0.015×10^{-4}	*m*
Thickness of the membrane	0.183×10^{-4}	*m*
Active area	1.024×10^{-3}	m^2

2.2. governing equations

2.2.1. Mass conservation equation

The mass conservation equation of PEMFC is as follows:

$$\frac{\partial(\varepsilon\varepsilon\rho)}{\partial t}+\nabla\cdot(\varepsilon\varepsilon\vec{u})=S_m \tag{1}$$

where, ρ is the fluid density (kg/m^3); ε is the porosity of porous media; $\vec{u}$ is the velocity vector (m) and S_m is the source term of quality.

2.2.2. Momentum conservation equation

The momentum conservation equation of PEMFC is as follows:

$$\frac{\partial(\varepsilon\varepsilon\vec{u})}{\partial t}+\nabla\cdot(\varepsilon\varepsilon\vec{u}\vec{u})=-\varepsilon\nabla p+\nabla\cdot(\varepsilon\varepsilon\nabla\vec{u})+S_u \tag{2}$$

where *P* represents pressure; μ is dynamic viscosity; and S_u represents the source term of power.

2.2.3. Energy conservation equation

The energy conservation equation of PEMFC is as follows:

$$(\varepsilon\rho c_p)_{eff}\frac{\partial T}{\partial t}+(\varepsilon\rho c_p)_{eff}(\vec{u}\nabla T)=\nabla\left(k_{eff}\nabla T\right)+S_e \tag{3}$$

where, c_p is the specific heat capacity of gas at constant pressure; T is the temperature; k_{eff} is the thermal conductivity; S_e is the source term of energy; and the subscript *eff* indicates the availability of porous media.

2.2.4. Species mass conservation equation

The species mass conservation equation of PEMFC is as follows:

$$\frac{\partial\left(\varepsilon c_k\right)}{\partial t}+\nabla\cdot\left(\varepsilon c_k\vec{u}\right)=\nabla\cdot\left(D_k^{eff}\nabla c_k\right)+S_k \tag{4}$$

where, c_k is the component concentration; D_k^{eff} is the effective diffusion coefficient of the components; S_k is the source term of component; and the subscript *k* represents the components, which are represented by hydrogen and water vapor at the anode, and oxygen, water vapor and nitrogen at the anode.

2.2.5. Current conservation equation

The current conservation equation of PEMFC is as follows:

$$\nabla\left(k_s^{eff}\nabla\phi_s\right)+S_{\phi s}=0 \tag{5}$$

$$\nabla\left(k_m^{eff}\nabla\phi_m\right)+S_{\phi m}=0 \tag{6}$$

where, k_s^{eff} is the conductivity of solid phase; k_m^{eff} is the conductivity of membrane phase; ϕ_s is the potential of solid phase; ϕ_m is the potential of membrane phase; $S_{\phi s}$ is the source term of electronic current; $S_{\phi m}$ is the source term of proton current.

2.2.6. Electrochemical reaction

According to the Bulter-Volmer equation, the electrochemical equation of PEMFC is as follows:

$$S_a = j_{a,ref}\left(\frac{C_{H_2}}{C_{H_{2,ref}}}\right)^{\lambda_a}\left(e^{\frac{\alpha_a F\eta_a}{RT}}-e^{-\frac{\alpha_c F\eta_a}{RT}}\right) \tag{7}$$

$$S_a = j_{c,ref}\left(\frac{C_{O_2}}{C_{O_{2,ref}}}\right)^{\lambda_c}\left(e^{\frac{\alpha_c F\eta_c}{RT}}-e^{-\frac{\alpha_a F\eta_c}{RT}}\right) \tag{8}$$

where, S_a is the source term of anode electrochemistry; S_c is the source term of cathode electrochemistry; $j_{a,ref}$ is the anode reference exchange current density; $j_{c,ref}$ is the cathode reference exchange current density; C_{H_2} and C_{O_2} are the molar concentrations of H_2 and O_2, respectively; $C_{H_2,ref}$ and $C_{O_2,ref}$ are the reference molar concentrations of H_2 and O_2, respectively; λ_a and λ_c are the anode and cathode concentration index and equal to 0.5 and 1 in this equation, respectively; and α_a, α_c are the anode and cathode transfer coefficients, respectively.

2.3. Boundary conditions

The boundary conditions required for calculation are defined as follows:

1. All internal boundaries are continuous;

2. There is no slip in all wall boundary conditions;

3. The exit of the flow channel does not have back pressure, but has the boundary condition of convective flow;

4. The outlet pressure of cathode and anode is set to 0;

5. The anode GDL boundaries facing the flow pattern ribs are set to zero electronic potential, and the corresponding boundaries at the cathode side are set to the cell potential. All other external boundaries are electrically isolating;

6. PEMFC is insulated from the environment

In addition, Table 2 lists the parameter settings related to the membrane, GDL, CL and reaction gases involved in the calculation process.

Table 2. Main parameters of the membrane, GDL, CL and reaction gases

parameter	Value	Unit
Electrical conductivity of the membrane	9	*S/m*
Porosity of GDLs	0.4	
Permeability of GDLs	1×10^{-13}	m^2
Electrical conductivity of GDLs	222	*S/m*
Anode inlet velocity	2	*m/s*
Cathode inlet velocity	2	*m/s*
The molar mass of H_2	0.002	*kg/mol*
The molar mass of N_2	0.028	*kg/mol*
The molar mass of H_2O	0.018	*kg/mol*
The molar mass of O_2	0.032	*kg/mol*
Binary diffusion coefficient of H_2-H_2O	1.1684×10^{-4}	m^2/s
Binary diffusion coefficient of N_2-H_2O	3.2682×10^{-5}	m^2/s
Binary diffusion coefficient of O_2-N_2	3.0466×10^{-5}	m^2/s
Binary diffusion coefficient of O_2-H_2O	3.5807×10^{-5}	m^2/s
Reference pressure	1.01×10^{-5}	*Pa*
Reference concentration of O_2	40.88	mol/m^3
Reference concentration of H_2	40.88	mol/m^3
Volume fraction of electrolyte phase	0.3	
Open volume fraction of gas diffusion in porous electrode	0.3	
Permeability of porous electrode	2×10^{-14}	m^2

2.4. Assumptions

In order to simplify the numerical simulation process, the following assumptions are made for the calculation model of PEMFCs [20-23]:

1. PEMFC operates in steady-state;
2. The gases of the anode (H_2) and cathode (O_2) are ideal and incompressible;
3. The reactant gas flow in the flow field is regarded as laminar flow;
4. All porous media (membrane, catalytic layer, gas diffusion layer) are regarded as isotropic and homogeneous;
5. Ignoring gravity effect;

6. The operating temperature of the battery is 80℃;
7. Symmetrical boundary conditions and non-slip conditions are supplied to GDL and catalyst layer.

2.5. Model validation

2.5.1. Mesh independence test

Figure 2 shows the polarization curves generated by the case with 5 rib floors and A-type hole arrangement under four different mesh quantities (123260, 141416, 192564, and 255072). It can be seen that the difference between the results produced by the latter three meshing schemes is acceptable, while the result from the first one is much lower. In order to simplify the research process and shorten the research time as much as possible on the premise of ensuring the accuracy, the second scheme was selected as the basis for the meshing of the model, and other models also adopted the same scheme in the meshing stage.

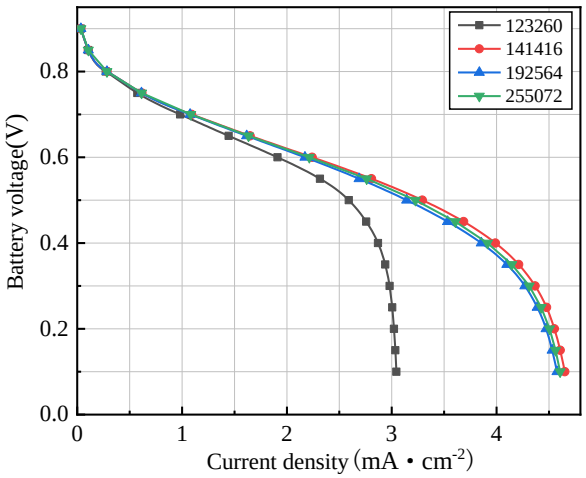

Figure 2. Polarization curves under four different mesh quantities

2.5.2. Experiment validation

In order to verify the reliability of the simulation models, we commissioned a professional manufacturer to process the PEMFC monomer including the circular bipolar plate used in this study, and tested it on the test platform, as shown in Figure 3. In this PEMFC monomer, the bipolar plate is composed of graphite material, and the membrane electrode assembly (MEA) is composed of a Nafion N-117 membrane from DuPont and TGP-H-120 PAN carbon paper from Toray (TORAYCA). Their main parameters are shown in Table 3. The data obtained from the experiment will be measured and saved by the IT8800 electronic load from ITECH.

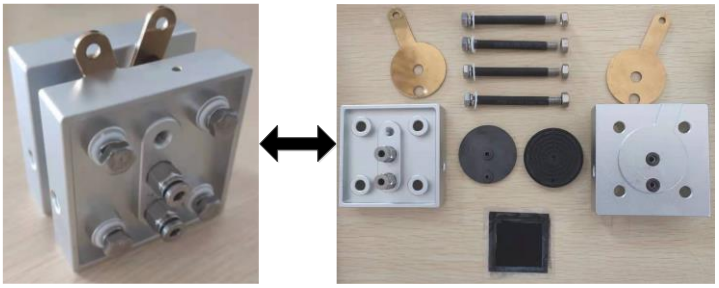

Figure 3. The PEMFC monomer including circular bipolar plate

Table 3. Main material parameters of Nafion N117 and TORAYCA TGP-H-120 PAN

Nafion N117	
parameter	**value**
Membrane density (μm)	360
Tensile modulus($g \cdot m^{-2}$)	249
Conductivity (MPa)	0.083
Strength of extension (MPa)	43/32 (vertical/horizontal)
Elongation at break (%)	225/310 (vertical/horizontal)
Tear strength ($g \cdot mm^{-1}$)	6000/6000 (vertical/horizontal)
TORAYCA TGP-H-120 PAN	
parameter	**value**
Volume density ($g \cdot m^{-3}$)	0.45
Porosity (%)	78
Surface roughness (μm)	8
Resistivity ($S \cdot m^{-1}$)	1250

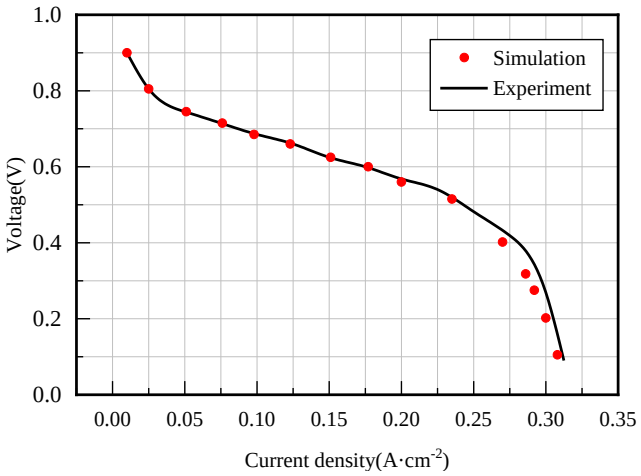

Figure 4. Comparison of the polarization curve between the simulation results and experimental data

Under the condition of trying to maintain the same operating environment, a three-dimensional PEMFC model with the radial flow channel structure was established and then simulated by the method of CFD in COMSOL Multiphysics. The polarization curves from the simulation results were compared

with the experimental results. Figure 4 shows that the experimental values are consistent with the simulated values. The findings indicate that the simulation model reflects the actual situation better and is reasonable to use for the optimization studies against radial flow channel structures.

3. RESULTS AND DISCUSSION

In order to investigate the effects of the number of rib floors and the number and arrangement of holes on the different ribs on the cell performance in the radial flow channel structure of circular bipolar plates, the difference between each scheme in terms of the oxygen distribution, water removal, cell output voltage and power density will be compared and analyzed respectively.

3.1. The number of rib floors

As shown in Figure 5, the geometric structures covered in this section are divided into four types according to the number of rib floors: 4 rib floors, 5 rib floors, 6 rib floors and 7 rib floors. The radius of the air inlet hole of all four schemes is 3.05 mm, and the size and distribution of the holes on the ribs at each floor are the same. The specific dimensional parameters of the models are listed in Table 1.

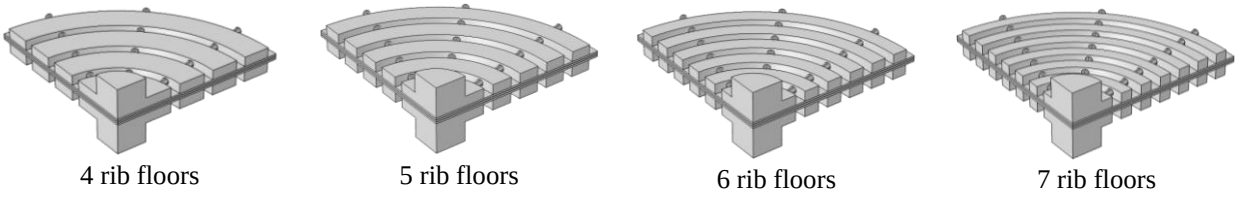

Figure 5. Radial flow channel structures with different numbers of rib floors

3.1.1. Effect on the cell output performance

Figure 6 shows the polarization curves and power density curves for the above four different rib floor schemes. As seen from the figure, at low current densities, the effect of the different rib floors on the voltage and power density generated by the cell is very small. However, the effect gradually increases at intermediate and high current densities. The figure also shows that when the number of rib floors increases from 4 to 5, the voltage and power density generated by the cell at the same current density increases accordingly. Likewise, 5 rib floors can bring a higher ultimate current density and maximum power density than 4 rib floors. As the number of rib floors continues to increase from 5, the performance of the cell starts to decrease instead. The flow channel structures with 6 and 7 rib floors produce rather lower voltage and power densities at the same current densities than the structures with 5 rib floors, but are still stronger than the structures with 4 rib floors.

In PEMFCs, electrons are generated in the membrane electrode assembly (MEA) and conducted to the external circuit through the ribs on the bipolar plate. The increase in the number of ribs can increase the contact area between the ribs and the MEA, which is beneficial to the conduction of current. However, with the increase in the number of ribs, the width of the flow channel decreases, thus leading to the reduction of the contact area between the flow field and the gas diffusion layer, which is not conducive to the full entry of the oxygen into the MEA to participate in the reaction and generate electrons. In other words, an optimal value occurs for the number of rib floors to maximize the current conduction of the bipolar plate while ensuring the full diffusion of oxygen to MEA to participate in reaction . Therefore, the selection of a reasonable number of rib floors is beneficial to enhancing the performance of the cell. From the polarization curves and current density curves, it can be observed that 5 rib floors is the best rib floor scheme in this study.

It is worth mentioning that Lian proposed a new radial flow channel structure and confirmed the improvement effect of this structure on fuel cell performance [24]. However, the flow channel structure of 5 rib floors in this study has a higher maximum power density ($0.12 W \cdot cm^{-2}$) than Lian's design ($0.11 W \cdot cm^{-2}$). In addition, the voltage and power density generated by the 5 rib floors structure are higher than those of his design under same current densities. Same results also appeared in the comparison with the radial flow channel structure proposed in the design of Cano-Andrade [15] and Friess [16]. It can be seen that this 5 rib floors structure offers a reference certain value in improving the fuel cell output performance.

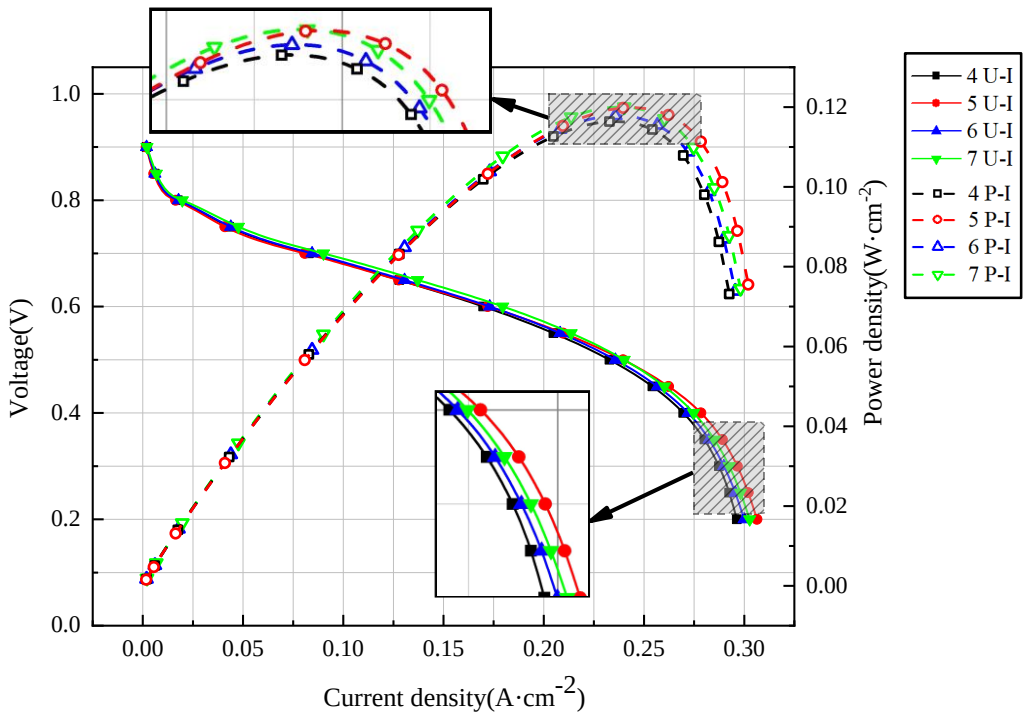

Figure 6. The polarization curves and power density curves for the above four different rib floor schemes

3.1.2. Oxygen distribution at the interface between GDL and CL

Figure 7 represents the oxygen distribution of the different schemes at the interface of the cathode GDL and CL under an operating voltage of 0.65V. As seen from the figure, the oxygen concentration at the interface decreases gradually along the inlet to the outlet of the flow field, which is mainly because when oxygen diffuses along the flow channel, it is also continuously involved in the reaction and consumed, thus its concentration decreases significantly when it reaches the outlet [25]. A comparison of the four different rib floor schemes showed that the oxygen concentration in the area closer to the rib holes within each layer of the flow channel is significantly higher than that at other locations, and this feature is more obvious in the outer layer of the flow channel. The reason for this phenomenon is that the distance between adjacent holes on the rib located on the outside of the flow field is large, and oxygen tends to gather only in the vicinity of the holes when diffusing through them into the flow channel, therefore, the area in the flow channel farther away from the holes is therefore not supplied with sufficient oxygen, which leads to a low oxygen concentration in this area. The uneven oxygen distribution leads to some areas of high oxygen concentration in the flow channels, and the electrochemical reaction occurring on the MEA corresponding to this area is relatively more intense, which eventually results in a large amount of heat that can cause irreversible damage to the MEA due to local overheating. As the number of rib floors increases, the inhomogeneity of the oxygen distribution becomes progressively more serious. In comparison, the oxygen distribution of the 4 rib floors is relatively the best among the four schemes, although its oxygen content, especially in the outermost flow channel, is still obviously nonuniform. In this regard, improving the uniformity of the oxygen distribution in the flow channel by optimizing the number and arrangement of holes will be the focus of the discussion in the next section.

For the four structures in this section alone, the average oxygen concentration difference within the flow field is maintained at about 6.5 mol/m^3 for the structures with 4 rib floors structure and 5 rib floors structure. The smaller the difference in the average oxygen concentration, the better the relative uniformity of oxygen distribution in the flow field. In contrast, the results obtained for the structures designed by Lian, Cano-Andrade and Friess are much larger. It can be seen that, in this aspect of oxygen distribution in the flow field, although the 4 and 5 rib floors structure still have huge potential for improvement, its existing effect on the optimization of oxygen distribution in the flow field is still relatively considerable.

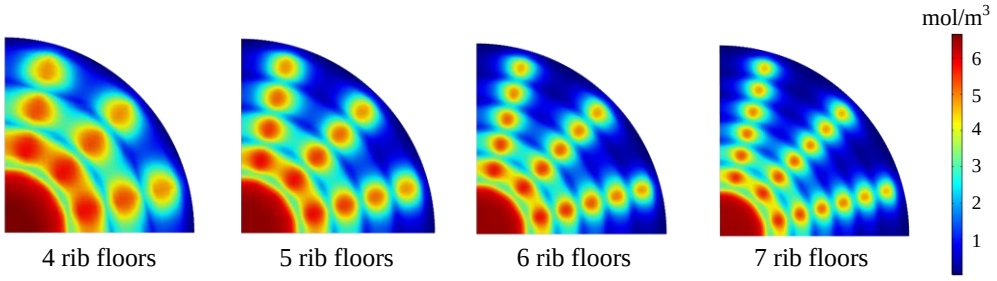

Figure 7. The oxygen distribution of different schemes at the interface of the cathode GDL and CL

3.1.3. Water distribution in the cathode flow channel

Figure 8 shows the water distribution of the different schemes in the cathode flow channel under an operating voltage of 0.65V. The water accumulated in the cathode flow channel mainly relies on the purge of the remaining reaction gas to discharge the flow field, therefore, the distribution of oxygen in the flow channel is highly contrasted with the distribution of water [26, 27]. As can be seen from the figure, the holes and their nearby areas have the lowest water content, and the more distant the location from the hole, the more serious the water aggregation. This behavior is mainly because that in the flow channels, more oxygen gathers near the holes, which also leads to a fuller purge of water by the oxygen. However, in the area far away from the holes, low-concentration oxygen is hindered from effectively purging the water after participating in the electrochemical reaction, so water gathers. A comparison of the different schemes shows that the overall water concentration in the flow channels gradually increases with the increase of the number of rib floors, and the area with water aggregation in each layer of the flow channel enlarges accordingly.

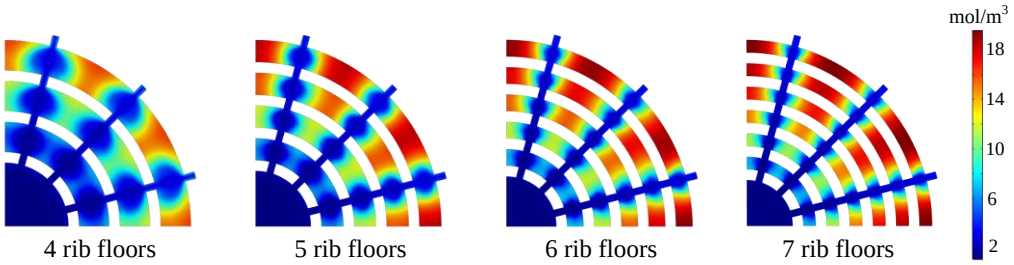

Figure 8. The water distribution of different schemes in the cathode flow field

3.1.4. Water distribution in the membrane

Figure 9 shows the water distribution of the different schemes in the membrane under an operating voltage of 0.65V. As shown in the figure, the trend of water distribution in the membrane is similar to that in the flow channel. The content of water in the membrane corresponding to the holes and their surrounding areas is lower, while the areas far from the holes experience the problem of water aggregation. High local water content in the membrane can easily lead to the occurrence of membrane flooding, while low water content can also easily cause membrane drying, which is not conducive to proton conduction, and may even cause membrane cracking, resulting in severe damage to the membrane. Comparing the four schemes, it can be found that although the uniformity of water distribution in the membrane is better in the flow field with 4 rib floors than in the other three schemes, the overall water content in the membrane of this scheme is too low, which is not conducive to proton conduction in the membrane and is the main reason for the poor electrochemical performance of the 4 rib floors scheme. In contrast, the 5 rib floors scheme is not as good as the 4 rib floors scheme in terms of water distribution uniformity, although it is significantly better than the 6 and 7 rib floors schemes. In addition, the overall water content of the 5 rib floors scheme is higher than that of the 4 rib floors scheme, and is not as over high as the 6 and 7 rib floor schemes. Therefore, in terms of the water content in the membrane, the 5

rib floors are the best choice among the four schemes, but the water distribution uniformity of it still needs to be improved. Zhu [28] conducted a study on the optimization of water content in the radial flow channel structure, and in his scheme, the average water content on the membrane was as low as 1.0 mol/m^3. In contrast, the average water content on the membrane with 5 rib floors structure is only about 0.46 mol/m^3, which is obviously better than Zhu's optimization result. In summary, in the subsequent structural optimization, the advantages of the flow field with 5 rib floors in terms of water content should be retained and its shortcomings in terms of water distribution uniformity should be improved through the design of the number and arrangement of rib holes.

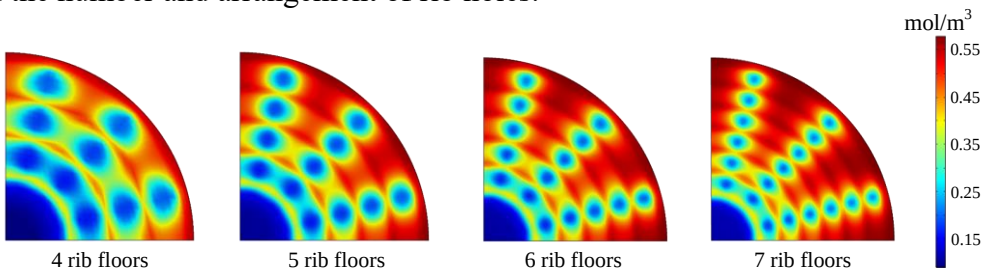

Figure 9. The water distribution of the different schemes in the membrane

3.2. The number and arrangement of holes on the different ribs

Based on the 5 rib floors, five different cases are designed for the number and arrangement of holes on the different ribs, as shown in Figure 10. Among them, A-type is the arrangement used in the previous section to study the 5 rib floors (3 holes for each floor), and the other four are the modified cases based on it. B-type and C-type are the progressive arrangements of the number of holes at each floor. D-type and E-type have similar hole arrangements, the main feature is that the number of holes in the ribs separated by one floor is the same, and the number of holes in the adjacent ribs differs by one. The specific number and distribution of the holes are shown in Table 4.

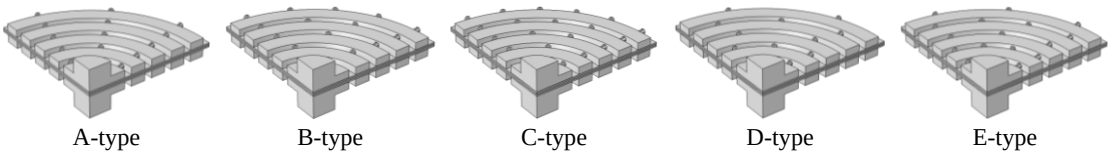

Figure 10. Radial flow field structures with different hole arrangements

Table 4. The number and distribution of the holes

Type	Hole arrangement from inside rib to outside rib	Total number of holes
A	3-3-3-3-3	15
B	1-2-3-4-5	15
C	2-3-4-5-6	20
D	2-3-2-3-2	12
E	3-4-3-4-3	17

3.2.1. Effect on the cell output performance

Figure 11 shows the polarization curves and power density curves for the five cases. The effects of different numbers and arrangements of rib holes on the output performance of the fuel cell are more obvious at intermediate and high current densities. In this region, the other four structures exhibit a greater increase in voltage and power density compared to the A-type structure because the holes on the adjacent ribs are distributed in the same radius direction in the A-type structure and this hole arrangement makes the rib extremely weak in guiding the reaction gas and shortens the residence time of the reaction gas in the annular flow channels at each floor. under the circumstances, the oxygen flows from the inlet to the outlet more like in a straight flow channel, and cannot be fully diffused in the annular flow channels, which leads to a low utilization rate of the reaction gas. In contrast, the irregular arrangement of holes enhances the diffusion effect of the oxygen in the flow channels enhanced, and the oxygen content is more uniform in the flow channels, which effectively alleviates the above problems. A comparison of A-type structure and D-type structure showed that including a higher number of holes does not increase the beneficial effect on the fuel cell output performance. Although the D-type structure has fewer holes than the A-type structure, the voltage and power density produced by the D-type structure under intermediate and high current densities is significantly better than that of the A-type structure. After the above analysis and comparison, it is clear that the arrangement and number of holes can indeed have an impact on the cell performance, however, choosing the proper arrangement of holes is more significant and has a more obvious improvement compared with increasing the number of holes.

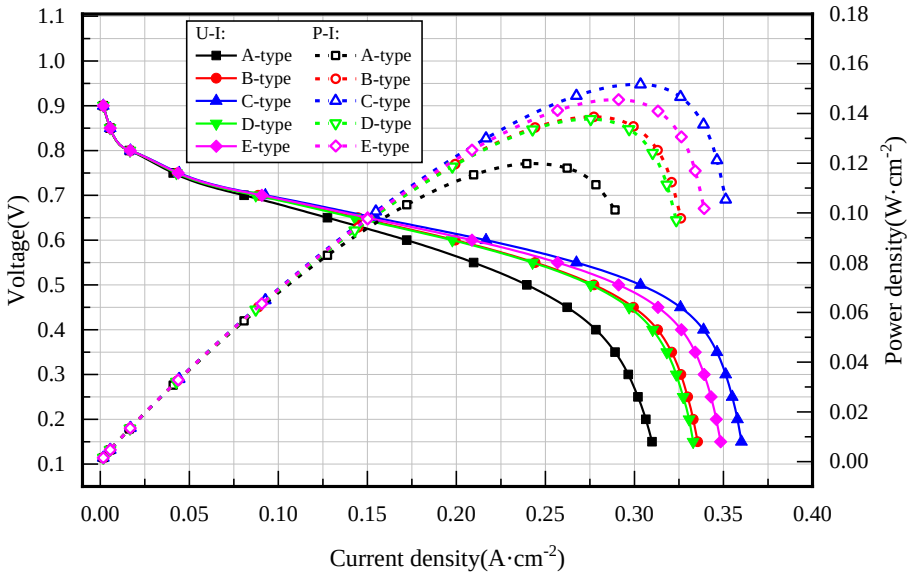

Figure 11. The polarization curves and power density curves for the five hole arrangement cases

On the other hand, B-type, C-type and D-type, E-type structures represent the two types of hole arrangements, respectively. The C-type structure exhibits the highest voltage and power density at intermediate and high current densities, followed by the E-type structure, and they are all substantially higher than those of the A-type structure. It can be seen that both arrangements are able to improve the output performance of the fuel cell. However, as shown in Figure 12, the improvement from B-type to

C-type is better than that from D-type to E-type for different current densities, and this effect is especially obvious in the voltage region under 0.7 V. Thus, optimizing the structure using the progressive distribution of each floor of holes is a more promising approach.

Similarly, the C-type structure, the most optimized of the five schemes in this section, was compared with the design of Lian [24]. The result showed that the C-type structure had a higher maximum power density ($0.15 W \cdot cm^{-2}$), and this value was also significantly improved over the scheme that only changed the number of rib floors. Thus, changing the number and arrangement of holes is certainly a more effective way to improve the performance of fuel cells.

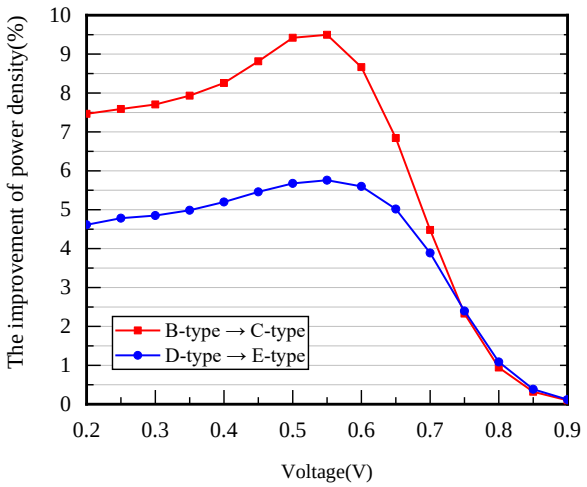

Figure 12. The improvement of power density between B-C types and D-E types

3.2.2. Oxygen distribution at the interface between GDL and CL

Figure 13 represents the oxygen distribution of different cases at the interface of the cathode GDL and CL under the operating voltage of 0.65V. Comparing the five holes arrangement cases, it can be seen that the concentration and distribution uniformity of oxygen within the last four cases, especially in the outer flow channels, appear to be significantly improved compared to the first case. In latter four cases, B-type and D-type still have an obvious low oxygen concentration region at the outermost position in the horizontal and vertical directions of the flow field, compared to C-type and E-type, which have higher oxygen concentrations in this region. In particular, C-type, which has the most uniform oxygen distribution among the four cases, is more conducive to the full diffusion of oxygen to all parts of the interface, even at the edge position of the flow field. In addition, Figure 14 also shows that C-type and E-type have lower concentration differences than B-type and D-type, and the oxygen concentration difference of C-type is the lowest in five cases.

In terms of the average oxygen concentration difference in the flow field, the C-type structure is maintained at about 6.2 mol/m^3, which is better than the result of Lian [24] and the 5 rib floors structure in the previous section. Besides, comparing this value with those of the straight flow field [29] and the serpentine flow field [30] under similar conditions, this value is still the smallest among them. For this

reason, it can be concluded that the optimized effect of the C-type structure on oxygen distribution is not only better in the radial flow field, but also in the comparison with the traditional flow field.

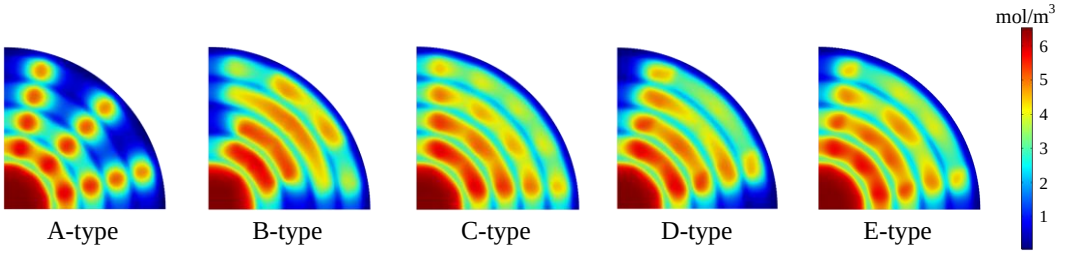

Figure 13. The oxygen distribution of five different cases at the interface of the cathode GDL and CL

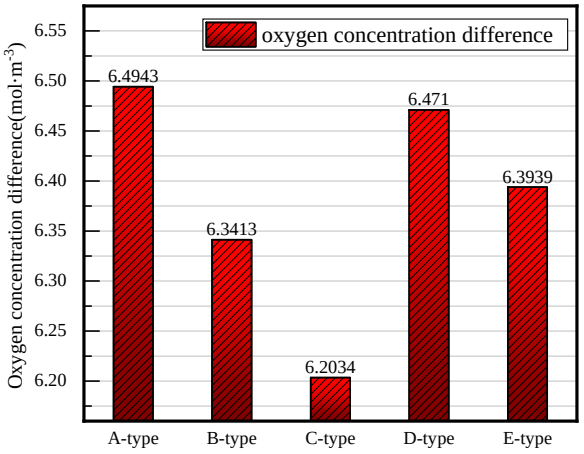

Figure 14. The oxygen concentration difference between five cases

3.2.3. Water distribution in the cathode flow channel

Figure 15 shows the water distribution of different cases in the cathode flow channel under the operating voltage of 0.65V. The uniformity of the water distribution within the flow channel of the A-type structure is the worst. This phenomenon is especially prominent in the outer flow channel. As mentioned previously, in the A-type case, the holes are arranged in the same radius direction, and the movement of gas from the inlet to the outlet is more like flowing along a straight flow channel, so the oxygen concentration is higher in the region close to the holes, and the water generated by the reaction here is more fully discharged from the flow field through the purging of oxygen. However, in the area far from the hole on both sides, the oxygen concentration is too low to enable effective purging of water, resulting in the water not being discharged smoothly through the holes, thus forming a high water content zone.

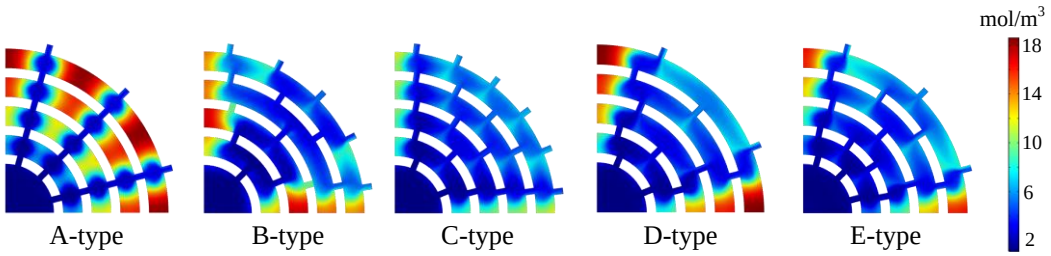

Figure 15. The water distribution of the five different cases in the cathode flow field

The four modified cases are intended to improve the convection effect of the fluid in the flow field by increasing the uniformity of the oxygen distribution, which in turn promotes the elimination of product water with the reaction gas. Figure 15 shows that the four modified cases indeed have a certain promotion effect on the elimination of water in the flow field compared to the A-type structure, and the area of high water concentration in the flow field is significantly reduced. A comparison of the last four cases in the figure showed that the water content in the border area on both sides of the fan-shaped flow field is higher than at other locations, which indicates that the water in the flow field is not sufficiently carried by oxygen here. Among the four cases, the C-type structure has the lowest degree of the above problem, and Figure 16 shows that the water concentration difference in such structure is also lower than that in other cases. Therefore, it can be considered that the distribution of water in the flow channel with C-type structure is more uniform, and the optimized effect is the best of the four.

After comparing the water concentration difference in the flow field of the C-type structure (10.65 mol/m^3) with that in the structure designed by Lian [24] and Zhu [28], it can be determined that the C-type structure has the lowest water concentration difference among them, and the highest water concentration that the C-type can reach in the flow field (11.28 mol/m^3) is also the lowest, which means that the water aggregation problem confronted by this type of the flow field is the smallest and the problem of flooding is the less likely to occur.

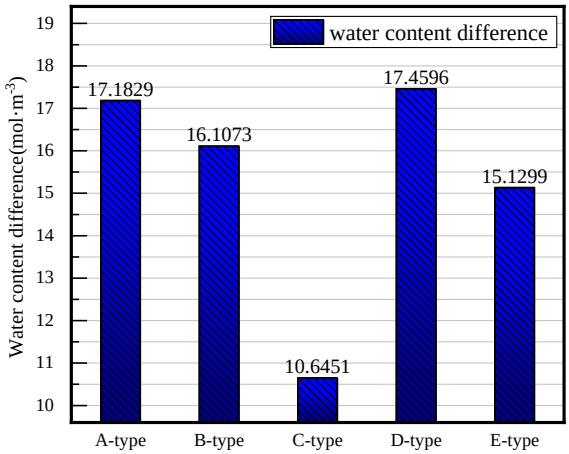

Figure 16. The water concentration difference between five cases

3.2.4. Water distribution in the membrane

Figure 17 shows the water distribution of different cases in the membrane under an operating voltage of 0.65V. For the A-type structure case, the overall water content in the membrane is higher and the water distribution is more uneven, resulting in a membrane prone to dry cracking or flooding, which seriously affects the service life of the membrane. In contrast, the four modified cases significantly reduced the area of high water concentration on the membrane. And the C-type structure has the minimum area with high water concentration and the most uniform water distribution. Combining all these characteristics indicates that the C-type case is the optimal hole arrangement.

Similarly, the difference in water concentration on the membrane was compared between the C-type structure and the scheme designed by Zhu [28], the result showed that the value was significantly lower in the flow field with the C-type structure (0.43 mol/m^3). In addition, the water concentration difference of the C-type structure is also slightly lower than that of only changing the number of rib floors (5 rib floors: 0.46 mol/m^3), which has a relatively smaller adverse effect on the membrane.

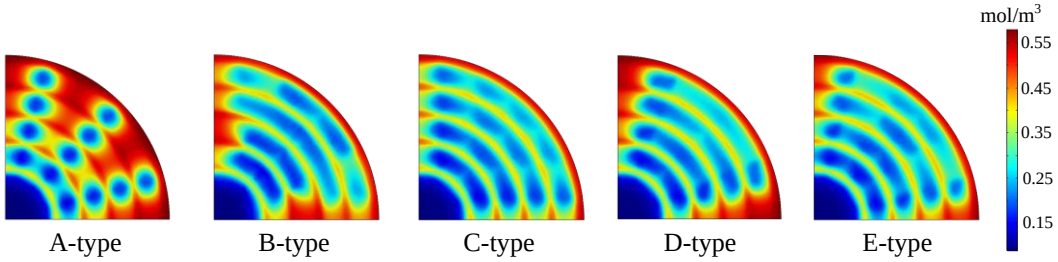

Figure 17. The water distribution of five different cases in the membrane

4. CONCLUSION

After a thorough investigation of previous research, a new radial flow channel structure on circular bipolar plates is proposed in this paper. In this structure, the number of rib floors and the number and arrangement of holes on the different ribs are selected as the key variables. In order to explore how these two key variables affect the performance of radial flow channel structures, PEMFC models with different arrangements of the mentioned above are established and then simulated through the CFD method. The ultimate aim of this study is to propose a comprehensive optimization scheme for this radial flow channel structure in terms of water distribution, oxygen distribution and fuel cell output performance by comparing and analyzing different simulation results.

Increasing the number of rib floors in the flow field does not effectively improve the output performance of the fuel cell. Among the four schemes compared in this study, the radial flow channel structure with 6 or 7 rib floors produced less voltage and power density than the structure with 5 rib floors at the same current densities. The same problem also appeared in the oxygen distribution at the interface between the cathode GDL and CL, and the water distribution in the flow channels or on the membrane. Although the structure with 5 rib floors is not as good as the structure with 4 rib floors in terms of oxygen distribution uniformity and water removal effect, it is obviously superior to the structure

with 6 or 7 rib floors, and the overall oxygen and water content in its flow field is higher than that with 4 rib floors, which is more conducive to the adequate reaction and wetting of the membrane.

In the analysis of the effect of the number of rib floors on the fuel cell performance, the arrangement of the holes on the ribs was consistent, and this arrangement caused poor gas conduction by the flow field and insufficient diffusion of oxygen, thereby leading to uneven distribution of the reaction gas in the annular flow channels, which prevented an adequate reaction and hindered the effective removal of water. In order to improve this problem, 4 new arrangements of holes on the ribs are proposed. The results show that when the number of holes on the ribs is arranged in increasing steps, the flow field becomes more effective in guiding the gas, the distribution of oxygen in the annular flow channel is more uniform, and the phenomenon of water accumulation in the flow channel is significantly reduced, which is more conducive to the improvement of fuel cell performance.

ACKNOWLEDGMENTS
This work was supported by the Major Science and Technology Innovation Project in Shandong Province (2018CXGC0803).

CONFLICT OF INTERESTS
The authors declare that there are no conflicts of interest regarding the publication of this article.

References

1. K.S. Choi, H.M. Kim and M.S. Moon, *Int. J. Hydrog. Energy*, 36(2) (2010) 1613.
2. L. Zhang, X. Chen, W. Wu and H. Gao, *Agricultural Engineering Technology*, 04 (2011) 15.
3. G.C. Steven, F.M. James and W.W. Fred, *J. Power Sources,* 86 (2000) 40.
4. F. Barbir, T. Gomez, *Int. J. Hydrog. Energy,* 22 (1997) 891.
5. G. Cacciola, V. Antonucci and S. Freni, *J. Power Sources,* 100 (2001) 67.
6. S. Dutta, S. Shimpalee and J.W. Van Zee, *J Appl Electrochem,* 30 (2000) 135.
7. W.K. Lee, J. Zee, S. Shimpalee and S. Dutta, Effect of humidity of PEM fuel cell performance. Part I. Experiments, *IMECE'99,* Nashville, Tennessee, USA, (1999) 359.
8. A. Su, Y.C. Chiu and F.B. Weng, *Int. J. Energy Res., 2*9 (2005) 409.
9. C. Huang, J. Lin, *J. Electrochem. Soc.,* 156 (2009) 178-B187.
10. R. Diethelm, J. Brun and B. Barp, Module for a fuel cell battery, US5270131 A, USA, (1993).
11. E. Batawi, High Temperature Fuel Cell, US5691075 A, USA, (1997).
12. A. Schuler, J. Schild, M. Jenne and P. Holoch, Fuel cell battery with an integrated heat exchanger, US7041406 B2, USA, (2006).
13. B. Doggwiler, M. Keller, Fuel cell battery with afterburning at the periphery of a cell stack, US6432567 B1, USA, (2002).
14. B. Doggwiler, E. Batawi, Fuel cell battery with a stack of planar cells, US6569554 B1, USA, (2003).
15. S. Cano-Andrade, A. Hernandez-Guerrero, M.R. Von Spakovsky, C.E. Damian-Ascencio and J.C. Rubio-Arana, *Energy,* 35 (2010) 920.
16. B.R. Friess, M. Hoorfar, *Int. J. Hydrog. Energy,* 37 (2012) 7719.
17. G. Vladimir, B.R. Frano and J.K. Neutzler, Fuel cell collector plates with improved mass transfer channels, US6551736 B1, USA, (2002).
18. I. Perez-Raya, A. Hernandez-Guerrero, F. Elizalde-Blancas, D. Juarez-Robles and L. Almanza-

Huerta, 3D Analysis of a New Radial Channel for PEMFCs and Comparison With a Traditional Channeled System, *Asme International Mechanical Engineering Congress & Exposition*, Vancouver, Canada, (2010) 899.
19. S. Ali, N. Behzad, M. Akbar, M. Kamyar and H.S. Amir, *Renew. Energ.,* 143 (2019) 1877.
20. A. Ramiar, A.H. Mahmoudi, Q. Esmaili and M. Abdollahzadeh, *Energy,* 94 (2016) 206.
21. B. Sezgin, D.G. Caglayan, Y. Devrim, T. Steenberg and I. Eroglu, *Int. J. Hydrog. Energy,* 41 (2016) 10001.
22. O. Bethoux, D. Candusso, F. Harel, C. Marchand and G. Coquery, *EUR PHYS J-APPL PHYS,* 54 (2011) 23412-1.
23. C.S. Xiong, M.J. Luo, B. Chen and T.U. Zheng-Kai, *Chinese Journal Of Power Sources,* 42 (2018) 230.
24. Y. Lian, M. Zheng, *Int. J. Ambient. Energy*, (2021) 1.
25. S. Hirano, J. Chen and S. Shimpalee, *ECS Meeting Abstracts*, (2016).
26. L. Hui, Y. Tang and Z. Wang, *J. Power Sources*, 178 (2008) 103.
27. X. Liu, H. Guo and C. Ma, *J. Power Sources*, 156 (2006) 267
28. W. Zhu, M. Zheng, *Int. J. Heat Mass Transf.*, 37 (2019) 733.
29. A.P. Manso, F.F. Marzo and J. Barranco, *Int. J. Hydrog. Energy*, 37 (2012) 15256.
30. L. Shi, M. Zheng, *EJST*, 1 (2019) 1.